Physical bounds on the all-spectrum transmission through periodic arrays: oblique incidence

Sjöberg, Daniel; Gustafsson, Mats; Larsson, Christer

2010

CODEN:LUTEDX/(TEAT-7199)/1-13/(2010)

Physical bounds on the all-spectrum transmission through periodic arrays: oblique incidence

Daniel Sjöberg, Mats Gustafsson, and Christer Larsson

Electromagnetic Theory
Department of Electrical and Information Technology
Lund University
Sweden

Daniel Sjöberg
Daniel.Sjoberg@eit.lth.se

Department of Electrical and Information Technology
Electromagnetic Theory
Lund University
P.O. Box 118
SE-221 00 Lund
Sweden

Christer Larsson
Christer.Larsson@saabgroup.com and Christer.Larsson@eit.lth.se

Saab Dynamics AB
SE-581 88 Linköping
Sweden

Department of Electrical and Information Technology
Electromagnetic Theory
Lund University
P.O. Box 118
SE-221 00 Lund
Sweden

Mats Gustafsson
Mats.Gustafsson@eit.lth.se

Department of Electrical and Information Technology
Electromagnetic Theory
Lund University
P.O. Box 118
SE-221 00 Lund
Sweden

Editor: Gerhard Kristensson

Abstract

The performance of a low-pass screen designed to block electromagnetic waves in a stop-band is shown to have an upper bound defined by the static electric and magnetic polarizability per unit area of the screen. The bound is easy to calculate for all angles of incidence and polarizations, and applies regardless of how complicated the screen's microstructure is. For a homogeneous dielectric sheet the bound for TM polarization is more restrictive than the bound for TE, but this is not generally true for a screen with microstructure. The results are verified by measurements and simulations of oblique transmission through an array of split ring resonators, printed on a dielectric substrate.

1 Introduction

In applications like radomes, spatial filters, polarizers, energy saving windows etc it is important to understand the transmission of electromagnetic waves through a planar screen of finite thickness, often having some microstructure. For normal incidence, it was shown in [11] that the blockage in transmission for a given nonmagnetic screen, integrated over all wavelengths, has an upper bound determined by the electric polarizability per unit area of the screen. In this paper, we generalize this result to include oblique incidence and magnetic materials, and investigate the dependence on polarization and angle of incidence for the incident wave.

Similar physical bounds restricting the performance of passive structures have been presented in several papers treating matching methods [5], finite size scatterers [10, 26–28], antennas [8, 9], absorbers [18], artificial magnetic ground planes [4], and metamaterials [7, 25, 29]. A common factor for all these bounds, is that the integrated electromagnetic interaction of the scatterer, antenna, or material, is bounded by the static properties of the system. This result is a consequence of assuming the system to be linear, causal, time translational invariant, and passive. Often, the static properties (such as polarizability) can be directly associated with properties such as the volume of the scatterer or similar. For instance, variational principles can be used to show that the electric polarizability of a given body, with or without inhomogeneous microstructure, is bounded above by the electric polarizability of a circumscribed metal body [12, 21].

The scattering of electromagnetic waves by an isotropic slab is well known and documented in many text books, see for instance [3, 17, 19]. The results have been generalized to homogeneous slabs of arbitrary bianisotropic materials [14, 23], but when the slab is inhomogeneous, for instance by loading it with metal inclusions, it is often necessary to resort to numerical methods to calculate reflection and transmission. The low-frequency limit for arbitrary slabs has been derived in [21], where it is seen that the low-frequency asymptotic is given by the electric and magnetic polarizability per unit area of the screen.

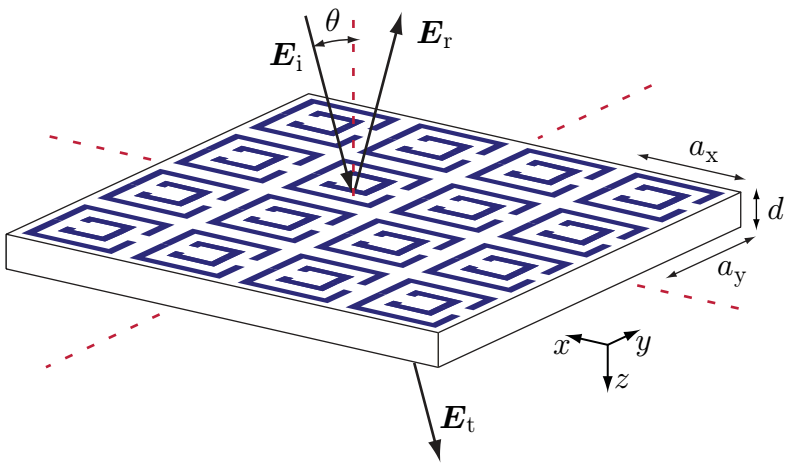

Figure 1: Geometry of the scattering problem.

2 Analyticity of the transmission coefficient

We start by investigating the analyticity of the transmission coefficient. A typical geometry of the problem is depicted in Fig. 1, where a plane wave is incident on a periodic structure with thickness d. The incident field has constant polarization $\boldsymbol{E}_0^{(\mathrm{i})}$ and unit propagation direction $\hat{\boldsymbol{k}}$, and can hence be written $\boldsymbol{E}^{(\mathrm{i})}(\boldsymbol{r},t) = \boldsymbol{E}_0^{(\mathrm{i})} f(t - \mathrm{c}_0^{-1}\hat{\boldsymbol{k}}\cdot\boldsymbol{r})$, where the time dependence satisfies $f(t) = 0$ for $t < 0$. Due to causality, the total field is zero until the plane wave has arrived, *i.e.*,

$$\boldsymbol{E}(\boldsymbol{r},t) = \boldsymbol{0} \quad \text{when} \quad t - \mathrm{c}_0^{-1}\hat{\boldsymbol{k}}\cdot\boldsymbol{r} < 0 \tag{2.1}$$

Since the geometry is periodic, we also have the translational invariance

$$\boldsymbol{E}(\boldsymbol{r}+\boldsymbol{r_n},t) = \boldsymbol{E}(\boldsymbol{r},t-\mathrm{c}_0^{-1}\hat{\boldsymbol{k}}\cdot\boldsymbol{r_n}) \tag{2.2}$$

where $\boldsymbol{r_n} = n_1\boldsymbol{a}_1 + n_2\boldsymbol{a}_2$, n_1 and n_2 taking integer values. The vectors $\boldsymbol{a}_1$ and $\boldsymbol{a}_2$ are lattice vectors in the xy-plane, forming the sides of the unit cell U, which has area $A = |\hat{\boldsymbol{z}}\cdot(\boldsymbol{a}_1\times\boldsymbol{a}_2)|$. Using the causality property (2.1), we can write the Fourier transform of the field as (where $k = \omega/\mathrm{c}_0$ is the wave number in vacuum, c_0 being the speed of light in vacuum and ω the angular frequency)

$$\begin{aligned}\boldsymbol{E}(\boldsymbol{r},k) = \int_{-\infty}^{\infty}\boldsymbol{E}(\boldsymbol{r},t)\mathrm{e}^{\mathrm{i}k\mathrm{c}_0 t}\,\mathrm{d}t &= \int_{\mathrm{c}_0^{-1}\hat{\boldsymbol{k}}\cdot\boldsymbol{r}}^{\infty}\boldsymbol{E}(\boldsymbol{r},t)\mathrm{e}^{\mathrm{i}k\mathrm{c}_0 t}\,\mathrm{d}t \\ &= \mathrm{e}^{\mathrm{i}k\hat{\boldsymbol{k}}\cdot\boldsymbol{r}}\underbrace{\int_0^{\infty}\boldsymbol{E}(\boldsymbol{r},t+\mathrm{c}_0^{-1}\hat{\boldsymbol{k}}\cdot\boldsymbol{r})\mathrm{e}^{\mathrm{i}k\mathrm{c}_0 t}\,\mathrm{d}t}_{\tilde{\boldsymbol{E}}(\boldsymbol{r},k)}\end{aligned} \tag{2.3}$$

The function $\boldsymbol{E}(\boldsymbol{r},t+\mathrm{c}_0^{-1}\hat{\boldsymbol{k}}\cdot\boldsymbol{r})$ is periodic in $\boldsymbol{r}$ due to the translational invariance (2.2). This property is inherited by $\tilde{\boldsymbol{E}}(\boldsymbol{r},k)$, which is also analytic in k for k in the

upper complex plane due to the lower integration limit, and satisfies the symmetry relation $\tilde{\boldsymbol{E}}(\boldsymbol{r}, k^*) = \tilde{\boldsymbol{E}}(\boldsymbol{r}, -k)^*$ since it is the Fourier transform of a real valued field. To summarize, the Fourier transformed field can be written using a Floquet-Bloch representation [2, 6, 20, 24]

$$\boldsymbol{E}(\boldsymbol{r}, k) = \mathrm{e}^{\mathrm{i}k\hat{\boldsymbol{k}}\cdot\boldsymbol{r}}\tilde{\boldsymbol{E}}(\boldsymbol{r}, k) = \mathrm{e}^{\mathrm{i}k_z z}\mathrm{e}^{\mathrm{i}\boldsymbol{k}_\mathrm{t}\cdot\boldsymbol{r}}\tilde{\boldsymbol{E}}(\boldsymbol{r}, k) \tag{2.4}$$

where $\tilde{\boldsymbol{E}}(\boldsymbol{r}, k)$ is periodic in the plane, and we split the incident wave vector in a transverse and longitudinal part, $k\hat{\boldsymbol{k}} = \boldsymbol{k}_\mathrm{t} + k_z\hat{\boldsymbol{z}}$. The Floquet modes of the field are defined as the Fourier series expansion of the periodic field at $z > d$, where d is the thickness of the structure:

$$\tilde{\boldsymbol{E}}(\boldsymbol{r}, k) = \sum_{\boldsymbol{n}} \boldsymbol{E}_{\boldsymbol{n}}(k)\mathrm{e}^{\mathrm{i}\boldsymbol{k}_{\boldsymbol{n}}\cdot\boldsymbol{r}}\mathrm{e}^{\mathrm{i}k_{z,\boldsymbol{n}}z}\mathrm{e}^{-\mathrm{i}k_z z} \tag{2.5}$$

where $\boldsymbol{k}_{\boldsymbol{n}} = n_1\boldsymbol{b}_1 + n_2\boldsymbol{b}_2$ and the longitudinal wave numbers are given by the relation $k_{z,\boldsymbol{n}}^2 = k^2 - |\boldsymbol{k}_\mathrm{t} + \boldsymbol{k}_{\boldsymbol{n}}|^2$. Note that $k_{z,\boldsymbol{n}}$ is imaginary for sufficiently large $\boldsymbol{n}$, indicating exponential damping. These are the evanescent modes, which hold purely reactive power and do not contribute to power transfer. The extra factor of $\mathrm{e}^{-\mathrm{i}k_z z}$ is necessary to cancel the corresponding factor multiplying $\tilde{\boldsymbol{E}}(\boldsymbol{r}, k)$ in (2.4). The vectors $\boldsymbol{b}_{1,2}$ are the reciprocal lattice vectors satisfying $\boldsymbol{a}_m \cdot \boldsymbol{b}_n = 2\pi\delta_{mn}$ [13]. If we had made the expansion at $z < 0$, the waves would be propagating in the negative z direction instead. The z component of the mode $\boldsymbol{E}_{\boldsymbol{n}}(k)$ can be computed from the xy components since $\boldsymbol{E}_{\boldsymbol{n}}(k)$ must be orthogonal to the total wave vector $\boldsymbol{k}_\mathrm{t} + \boldsymbol{k}_{\boldsymbol{n}} + k_{z,\boldsymbol{n}}\hat{\boldsymbol{z}}$. Thus, it is sufficient to consider only the transverse components of the modes in order to discuss the transmission. The 2×2 transmission matrix $\mathbf{T}(k)$ is then defined by the transverse components of the zeroth mode as

$$\boldsymbol{E}_{\boldsymbol{0},\mathrm{t}}(k) = \mathbf{T}(k) \cdot \boldsymbol{E}_{0,\mathrm{t}}^{(\mathrm{i})} \tag{2.6}$$

Since $\tilde{\boldsymbol{E}}(\boldsymbol{r}, k)$ is analytic in k for all $\boldsymbol{r}$, then so is

$$\boldsymbol{E}_{\boldsymbol{0},\mathrm{t}}(k) = \frac{1}{|U|}\int_U \tilde{\boldsymbol{E}}_\mathrm{t}(\boldsymbol{r}, k)\,\mathrm{d}S \tag{2.7}$$

and hence also $\mathbf{T}(k)$. In the following, we discuss the implications of the analyticity of the diagonal element $T(k) = \boldsymbol{E}_{0,\mathrm{t}}^{(\mathrm{i})} \cdot \mathbf{T}(k) \cdot \boldsymbol{E}_{0,\mathrm{t}}^{(\mathrm{i})}/|\boldsymbol{E}_{0,\mathrm{t}}^{(\mathrm{i})}|^2$, corresponding to the co-polarized transmitted field.

3 Physical bound

Following [11], we take into account that the transmission coefficient is a transfer function, and hence may have some zeros $\{k_n\}_{n=1}^N$ in the upper half plane. To obtain a function where all poles and zeros are in the lower half plane, we multiply $T(k)$ by a Blaschke product and take the logarithm, which produces the Herglotz function

(analytic mapping of the upper half plane to itself, satisfying $h(k) = -h^*(-k^*)$ [1, 16])

$$h(k) = -\mathrm{i}\ln\left(T(k)\prod_{n=1}^{N}\frac{k_n^* - k}{k_n - k}\right) \tag{3.1}$$

The Blaschke product multiplying $T(k)$ in the expression above has unit amplitude on the real line $\mathrm{Im}(k) = 0$, and serves the purpose of shifting all possible zeros k_n of $T(k)$ in the upper plane to zeros k_n^* in the lower plane, thereby making $h(k)$ equivalent to a minimum phase function. In [1], it is shown that the function $h(k)/k^2$ satisfies the following sum rule (with additional assumptions this can also be shown using Cauchy integrals as in [16, 26–28])

$$\frac{2}{\pi}\int_0^\infty \frac{\mathrm{Im}\, h(k)}{k^2}\,\mathrm{d}k = \lim_{k\to 0}\frac{T(k)-1}{\mathrm{i}k} - \lim_{k\to\infty}\mathrm{Im}\,\frac{\ln(T(k))}{k} + 2\sum_{n=1}^{N}\mathrm{Im}\,\frac{1}{k_n} \tag{3.2}$$

The imaginary part of $1/k_n$ is negative for all $n = 1, \ldots, N$. The high frequency limit corresponds to the asymptotic phase delay, and can be represented by introducing the high frequency refractive index n_∞ as

$$\begin{aligned}\mathrm{Im}\,\frac{\ln(T(k))}{k} &\to \frac{\sqrt{k^2 n_\infty^2 - |\boldsymbol{k}_\mathrm{t}|^2} - \sqrt{k^2 - |\boldsymbol{k}_\mathrm{t}|^2}}{k} d \\ &= \left(\sqrt{n_\infty^2 - \sin^2\theta} - \cos\theta\right) d, \quad k\to\infty\end{aligned} \tag{3.3}$$

The low frequency limit of the transmission coefficient for a low-pass screen can be written [21]

$$\begin{aligned}\mathbf{T} = \mathbf{1} + \frac{\mathrm{i}k}{2}\Bigg\{&\eta_0^{-1}\mathbf{Z}_0\cdot\left[\frac{\boldsymbol{\gamma}_\mathrm{ett}}{A} + \frac{\boldsymbol{k}_\mathrm{t}'\boldsymbol{k}_\mathrm{t}'}{k^2}\frac{\gamma_{\mathrm{m}zz}}{A}\right] + \left[-\hat{\boldsymbol{z}}\times\frac{\boldsymbol{\gamma}_\mathrm{mtt}}{A}\cdot\hat{\boldsymbol{z}}\times + \frac{\boldsymbol{k}_\mathrm{t}\boldsymbol{k}_\mathrm{t}}{k^2}\frac{\gamma_{\mathrm{e}zz}}{A}\right]\cdot\mathbf{Z}_0^{-1}\eta_0 \\ &+ \mathbf{Z}_0\cdot\left[\frac{\boldsymbol{k}_\mathrm{t}'}{k}\frac{\boldsymbol{\gamma}_{\mathrm{m}z}}{A} - \frac{\boldsymbol{\gamma}_\mathrm{et}}{A}\frac{\boldsymbol{k}_\mathrm{t}'}{k}\right]\cdot\hat{\boldsymbol{z}}\times\mathbf{Z}_0^{-1} + \hat{\boldsymbol{z}}\times\left[\frac{\boldsymbol{k}_\mathrm{t}'}{k}\frac{\boldsymbol{\gamma}_{\mathrm{e}z}}{A} - \frac{\boldsymbol{\gamma}_\mathrm{mt}}{A}\frac{\boldsymbol{k}_\mathrm{t}'}{k}\right]\Bigg\} + \mathrm{o}(k)\end{aligned} \tag{3.4}$$

where $\boldsymbol{k}_\mathrm{t}$ is the transverse wave number, and the wave impedance dyadic in the surrounding free space is

$$\mathbf{Z}_0 = \eta_0\cos\theta\frac{\boldsymbol{k}_\mathrm{t}\boldsymbol{k}_\mathrm{t}}{|\boldsymbol{k}_\mathrm{t}|^2} + \frac{\eta_0}{\cos\theta}\frac{\boldsymbol{k}_\mathrm{t}'\boldsymbol{k}_\mathrm{t}'}{|\boldsymbol{k}_\mathrm{t}'|^2} \tag{3.5}$$

where $\boldsymbol{k}_\mathrm{t}' = \hat{\boldsymbol{z}}\times\boldsymbol{k}_\mathrm{t}$ and $\sin\theta = |\boldsymbol{k}_\mathrm{t}|/k$ represents the angle of incidence, see Fig. 1. The electric and magnetic polarizability matrices $\boldsymbol{\gamma}_\mathrm{e}$ and $\boldsymbol{\gamma}_\mathrm{m}$ give the total electric and magnetic dipole moment per unit area induced in the screen when subjected to homogeneous fields $\boldsymbol{E}_0$ and $\boldsymbol{H}_0$ as $\boldsymbol{p}/A = \epsilon_0\boldsymbol{\gamma}_\mathrm{e}\cdot\boldsymbol{E}_0/A$ and $\boldsymbol{m}/A = \boldsymbol{\gamma}_\mathrm{m}\cdot\boldsymbol{H}_0/A$, respectively. The matrices are decomposed as (where $\boldsymbol{\gamma}_\mathrm{ett}$ can be represented as a 2×2 matrix, $\boldsymbol{\gamma}_\mathrm{et}$ and $\boldsymbol{\gamma}_{\mathrm{e}z}$ are vectors in the xy plane, and $\gamma_{\mathrm{e}zz}$ is a scalar)

$$\begin{aligned}\boldsymbol{\gamma}_\mathrm{e}\cdot\boldsymbol{E} &= (\boldsymbol{\gamma}_\mathrm{ett} + \boldsymbol{\gamma}_\mathrm{et}\hat{\boldsymbol{z}} + \hat{\boldsymbol{z}}\boldsymbol{\gamma}_{\mathrm{e}z} + \gamma_{\mathrm{e}zz}\hat{\boldsymbol{z}}\hat{\boldsymbol{z}})\cdot(\boldsymbol{E}_\mathrm{t} + \hat{\boldsymbol{z}}E_z) \\ &= \boldsymbol{\gamma}_\mathrm{ett}\cdot\boldsymbol{E}_\mathrm{t} + \boldsymbol{\gamma}_\mathrm{et}E_z + \hat{\boldsymbol{z}}(\boldsymbol{\gamma}_{\mathrm{e}z}\cdot\boldsymbol{E}_\mathrm{t} + \gamma_{\mathrm{e}zz}E_z)\end{aligned} \tag{3.6}$$

and similarly for $\boldsymbol{\gamma}_{\mathrm{m}}$. Let the plane of incidence coincide with the xz plane so that $\boldsymbol{k}_{\mathrm{t}} = k\sin\theta\hat{\boldsymbol{x}}$, and assume for simplicity that the polarizability matrices are diagonal in the xyz coordinate system in Fig. 1, *i.e.*, $\boldsymbol{\gamma}_{\mathrm{e}z} = \boldsymbol{\gamma}_{\mathrm{et}} = \boldsymbol{\gamma}_{\mathrm{m}z} = \boldsymbol{\gamma}_{\mathrm{mt}} = \mathbf{0}$, $\boldsymbol{\gamma}_{\mathrm{ett}} = \gamma_{\mathrm{e}xx}\hat{\boldsymbol{x}}\hat{\boldsymbol{x}} + \gamma_{\mathrm{e}yy}\hat{\boldsymbol{y}}\hat{\boldsymbol{y}}$, and $\boldsymbol{\gamma}_{\mathrm{mtt}} = \gamma_{\mathrm{m}xx}\hat{\boldsymbol{x}}\hat{\boldsymbol{x}} + \gamma_{\mathrm{m}yy}\hat{\boldsymbol{y}}\hat{\boldsymbol{y}}$. The factor multiplying $\mathrm{i}k/2$ in (3.4) then simplifies considerably and we have

$$\mathbf{T} = \mathbf{1} + \frac{\mathrm{i}k}{2A}\Bigg\{ \left[\cos\theta\gamma_{\mathrm{e}xx} + \frac{\sin^2\theta}{\cos\theta}\gamma_{\mathrm{e}zz} + \frac{\gamma_{\mathrm{m}yy}}{\cos\theta}\right]\hat{\boldsymbol{x}}\hat{\boldsymbol{x}} + \left[\frac{\gamma_{\mathrm{e}yy}}{\cos\theta} + \cos\theta\gamma_{\mathrm{m}xx} + \frac{\sin^2\theta}{\cos\theta}\gamma_{\mathrm{m}zz}\right]\hat{\boldsymbol{y}}\hat{\boldsymbol{y}}\Bigg\} + \mathrm{o}(k) \quad (3.7)$$

Introducing the total polarizability

$$\gamma(\theta) = \begin{cases} \gamma_{\mathrm{e}xx}\cos^2\theta + \gamma_{\mathrm{e}zz}\sin^2\theta + \gamma_{\mathrm{m}yy} & \mathrm{TM} \\ \gamma_{\mathrm{e}yy} + \gamma_{\mathrm{m}xx}\cos^2\theta + \gamma_{\mathrm{m}zz}\sin^2\theta & \mathrm{TE} \end{cases} \quad (3.8)$$

and using (3.3), (3.7), and that $\operatorname{Im} 1/k_n < 0$, the sum rule (3.2) can now be written as the physical bound

$$\frac{2}{\pi}\int_0^\infty \frac{1}{k^2}\ln\frac{1}{|T(k)|}\,\mathrm{d}k = \frac{1}{\pi^2}\int_0^\infty \ln\frac{1}{|T(\lambda)|}\,\mathrm{d}\lambda \le \frac{\gamma(\theta)}{2A\cos\theta} - \left(\sqrt{n_\infty^2 - \sin^2\theta} - \cos\theta\right)d \quad (3.9)$$

which is our main result. Here, $\lambda = 2\pi/k$ is the wavelength, and we reuse the symbol T for the transmission as a function of λ. To express this in terms of bandwidth and transmission level, we estimate the integral as in [11] to find

$$\int_0^\infty \ln\frac{1}{|T(\lambda)|}\,\mathrm{d}\lambda \ge \int_{\lambda_1}^{\lambda_2} \ln\frac{1}{|T(\lambda)|}\,\mathrm{d}\lambda \ge (\lambda_2 - \lambda_1)\ln\frac{1}{T_0} \quad (3.10)$$

where $T_0 = \max_{\lambda\in[\lambda_1,\lambda_2]}|T(\lambda)|$ is the maximum transmission in the stop band $[\lambda_1, \lambda_2]$. This implies

$$B\ln\frac{1}{T_0} \le \frac{\pi^2\gamma(\theta)}{2A\lambda_0\cos\theta} - \left(\sqrt{n_\infty^2 - \sin^2\theta} - \cos\theta\right)\frac{\pi^2 d}{\lambda_0} \quad (3.11)$$

where $\lambda_0 = (\lambda_1 + \lambda_2)/2$ is the center wavelength, and $B = (\lambda_2 - \lambda_1)/\lambda_0$ is the fractional bandwidth.

4 Calculation of polarizabilities

The electric polarizability can be calculated from the solution of the static problem

$$\nabla\times\boldsymbol{E} = \mathbf{0}, \quad \nabla\cdot\boldsymbol{D} = 0, \quad \boldsymbol{D}(\boldsymbol{r}) = \epsilon_0\boldsymbol{\epsilon}(\boldsymbol{r})\cdot\boldsymbol{E}(\boldsymbol{r}) \quad (4.1)$$

with periodic boundary conditions in the xy-plane, and the requirement $\boldsymbol{E} \to \boldsymbol{E}_0$ as $z \to \pm\infty$. Since $\boldsymbol{\epsilon}(\boldsymbol{r})$ is a matrix, this formulation includes anisotropic materials. The polarizability is then given by

$$\boldsymbol{\gamma}_{\mathrm{e}} \cdot \boldsymbol{E}_0 = \int (\boldsymbol{\epsilon}(\boldsymbol{r}) - \mathbf{1}) \cdot \boldsymbol{E}(\boldsymbol{r}) \, \mathrm{d}V \tag{4.2}$$

The same procedure applies to the magnetic polarizability $\boldsymbol{\gamma}_{\mathrm{m}}$, substituting $\boldsymbol{\epsilon}$ with $\boldsymbol{\mu}$. The difference between the two cases arises only for PEC structures, where the electric boundary condition is $\hat{\boldsymbol{n}} \times \boldsymbol{E} = \mathbf{0}$, and the magnetic is $\hat{\boldsymbol{n}} \cdot \boldsymbol{B} = 0$. Further information on the calculation of the polarizabilities can be found in [21]. Using variational principles, the polarizabilities can be given upper and lower bounds [22].

5 Examples

We illustrate the bound (3.9) with two nonmagnetic examples, *i.e.*, $\boldsymbol{\gamma}_{\mathrm{m}} = \mathbf{0}$ in both cases. The first is theoretical transmission through a dielectric sheet, and the second is measured and simulated transmission through a periodic array of split ring resonators. In Figs. 2 and 6, the left and right hand sides of (3.9) are scaled by $\cos\theta$ to avoid the singularity at grazing incidence.

5.1 Dielectric sheet

For a dielectric, nonmagnetic sheet with relative permittivity $\epsilon_{\mathrm{r}}(k)$, the transmission coefficient is [3]

$$T(k) = \frac{(1 - r_0(k)^2)\mathrm{e}^{\mathrm{i}(\beta(k) - \beta_0(k))d}}{1 - r_0(k)^2 \mathrm{e}^{\mathrm{i}2\beta(k)d}} \tag{5.1}$$

where the wave numbers in the material and in the surrounding free space are given by $\beta(k)^2 = k^2(\epsilon_{\mathrm{r}}(k) - \sin^2\theta)$ and $\beta_0(k) = k\cos\theta$, respectively, and the interface reflection coefficient is $r_0 = (Z - Z_0)/(Z + Z_0)$ with $Z = \eta_0 k/\beta$ and $Z_0 = \eta_0/\cos\theta$ for TE polarization, and $Z = \eta_0\beta/(\epsilon_{\mathrm{r}}(k)k)$ and $Z_0 = \eta_0\cos\theta$ for TM polarization. The static polarizability factors are [21]

$$\gamma_{\mathrm{e}xx} = \gamma_{\mathrm{e}yy} = Ad(\epsilon_{\mathrm{r}}(0) - 1), \quad \gamma_{\mathrm{e}zz} = Ad(1 - \epsilon_{\mathrm{r}}(0)^{-1}) \tag{5.2}$$

whereas the high frequency refractive index is $n_\infty = \sqrt{\epsilon_\infty}$, where $\epsilon_\infty = \lim_{k\to\infty} \epsilon_{\mathrm{r}}(k)$ is the high frequency limit of the relative permittivity. From (3.8) it is seen that since $1 - \epsilon_{\mathrm{r}}(0)^{-1} < \epsilon_{\mathrm{r}}(0) - 1$, the polarizability factor for TM polarization is always less than for TE, which demonstrates that the maximum transmission blockage is always less for TM polarization.

In Fig. 2 we have computed the integral in the left hand side of (3.9) for a 0.3 mm thick dielectric sheet with two different relative permittivities: one frequency independent $\epsilon_{\mathrm{r}} = 4.35$ (solid lines), and one frequency dependent $\epsilon_{\mathrm{r}}(k) = 1 + (4.35 - 1)/(1 - \mathrm{i}k/k_{\mathrm{c}})$ (dashed lines). The cutoff wavenumber was chosen as $k_{\mathrm{c}} = 2\pi/1\,\mu\mathrm{m}$ so that $\epsilon_{\mathrm{r}}(k) \approx 4.35$ when $\lambda \gg 1\,\mu\mathrm{m}$, *i.e.*, in the region where the sheet is in the

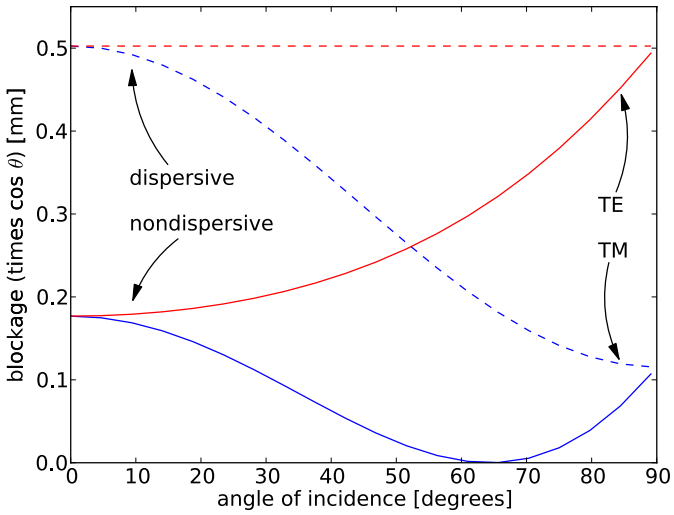

Figure 2: The integrated transmission blockage and its bounds (left and right hand side of (3.9) times $\cos\theta$) for a 0.3 mm dielectric sheet. Solid lines are for constant (nondispersive) relative permittivity $\epsilon_{\mathrm{r}} = 4.35$, dashed lines are for frequency dependent (dispersive) relative permittivity $\epsilon_{\mathrm{r}}(k) = 1 + (4.35 - 1)/(1 - \mathrm{i}k/k_{\mathrm{c}})$, using $k_{\mathrm{c}} = 2\pi/(1\,\mu\mathrm{m})$. The bounds are exactly on top of the simulated transmission blockage. Note the zero transmission blockage for nondispersive case in TM polarization at 64°, corresponding to the Brewster angle.

order of a few wavelengths, and the high frequency asymptote is $n_\infty = 1$. In all cases, the integrated transmission blockage is exactly on top of the bound.

For the nondispersive permittivity, the Brewster angle phenomenon is clearly seen in Fig. 2: at the Brewster angle $\theta_{\mathrm{B}} = \arctan(\sqrt{\epsilon_{\mathrm{r}}}) = 64°$, the interface reflection coefficient r_0 for TM polarization is exactly zero, and the transmission coefficient has unit amplitude $|T| = 1$. With a frequency independent material, the Brewster angle is the same for all frequencies and hence the total transmission blockage is zero for TM polarization at this angle.

The Brewster angle effect disappears when considering the frequency dependent material (dashed lines in Fig. 2), since this angle now varies with frequency. It is further seen that the overall level of transmission blockage is increased for the dispersive material, particularly for normal incidence, and the TE result is independent of the angle of incidence (except for the scaling with $\cos\theta$), due to the high frequency response being tuned to vacuum.

It is interesting to note that we can lower the cutoff frequency k_{c} to a value corresponding to wavelengths much longer than the sheet thickness d without changing the dashed lines in Fig. 2 (not shown). Indeed, since $|r_0| < 1$ for all frequencies it is seen from (5.1) that $T(k)$ does not have any zeros, and the bound (3.9) is actually an *equality* for the dielectric sheet. This means the total transmission blockage is determined exactly by the low- and high-frequency asymptotics on the right hand

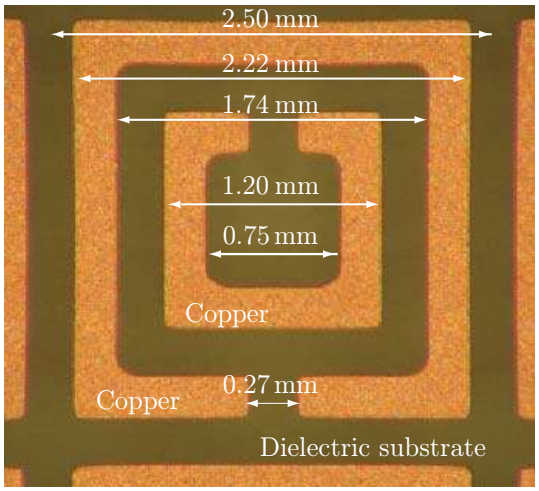

Figure 3: Geometry of the metal split ring resonators on a 0.3 mm thick FR4 substrate with $\epsilon_r = 4.35$. The total sheet has $240 \times 240 = 57\,600$ unit cells, and is 60 cm $\times$ 60 cm.

side of (3.9), which also explains why the simulations equal the bounds in Fig. 2.

5.2 Array of split ring resonators

Measurements were performed on the same sheet of printed metal split ring resonators on a thin FR4 substrate as in [11]. The unit cell geometry is depicted in Fig. 3. The sheet was mounted in a cardboard frame to provide mechanical stability, and the transmission through the sheet was measured for five angles of incidence: 0°, 23°, 34°, 45°, and 67°.

The measurements were made using pairs of wideband ridged horn antennas, separated by 0.6 m with the sheet in between, see Fig. 4. Keeping the sheet fixed, the antennas were moved to obtain the different polarizations and angles of incidence. To cover a wide frequency range, two pairs of horns were used, one for $[1, 22]$ GHz and one for $[16, 40]$ GHz. The sheet measurements were normalized by measurements with the sheet absent, and a 2 ns time-gating was applied in the time-domain to minimize the influence from the background, which reduces the useful frequency range to $[2, 38]$ GHz. The plane of incidence was horizontal, making the vertical-to-vertical (VV) measurement correspond to TE polarization, and the horizontal-to-horizontal (HH) measurement correspond to TM polarization.

The sheet was also simulated using the commercial program CST Microwave Studio for the frequency range $[0.2, 40]$ GHz for both polarizations and the same angles of incidence as the measurements. The simulated results are compared with measured results in Fig. 5 for $\theta = 23°$ and 67°, and it is seen that the agreement is very good.

In [11], the transverse polarizabilities of the sheet were computed to $\gamma_{exx}/A = 7.2$ mm and $\gamma_{eyy}/A = 7.1$ mm. The longitudinal polarizability can be estimated by

Figure 4: Measurement setup for oblique incidence on an array of split ring resonators. The sheet was oriented with the gaps in the split rings along the vertical direction.

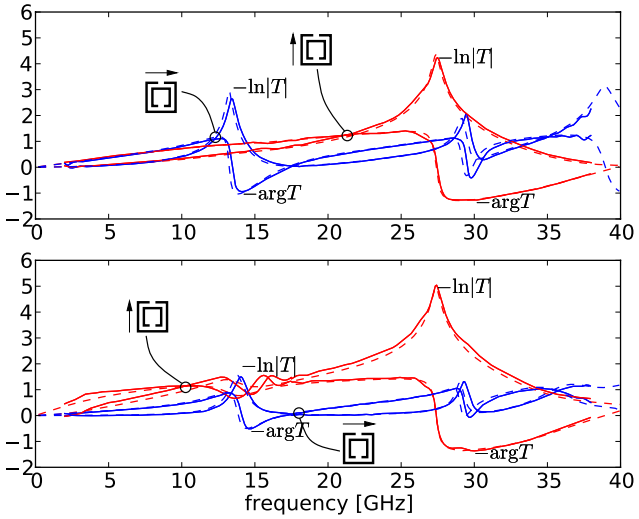

Figure 5: The real and imaginary parts of $-\ln T = -\ln|T| - \mathrm{i}\arg T$ for $\theta = 23°$ (upper graph) and 67° (lower graph). Solid lines are measurements, dashed lines are simulations.

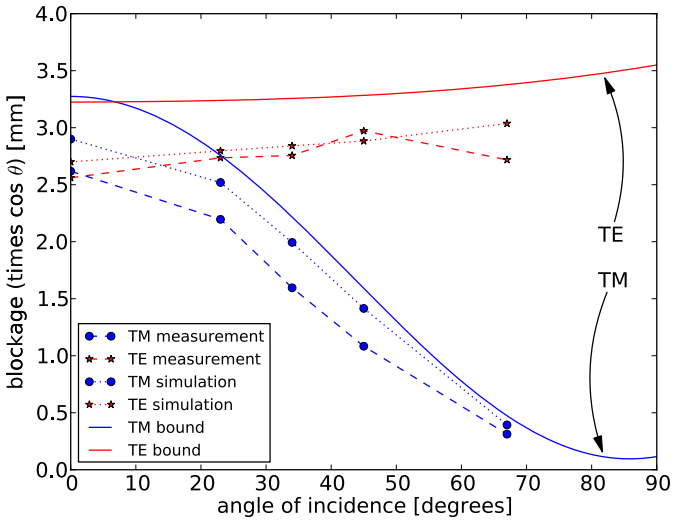

Figure 6: The integrated transmission blockage (left hand side of (3.9) times $\cos\theta$) for measurements (dashed lines) and simulations (dotted lines) of the sheet in Fig. 3. The bounds (right hand side of (3.9) times $\cos\theta$) are solid lines.

the polarizability of the substrate, $\gamma_{ezz}/A = (1-\epsilon_{\mathrm{r}}^{-1})d = 0.23\,\mathrm{mm}$. The measured and simulated transmission coefficients were then used to calculate the integral in the left hand side of (3.9), and the result is depicted in Fig. 6, together with the bounds in the right hand side of (3.9). It is seen that the measured and simulated results for the TE polarization are below its corresponding bound, but exceeds the bound of the TM polarization. The trends correspond well to the calculations for a pure dielectric substrate in Fig. 2, but the amplitude of the computed integrals and bounds are an order of magnitude larger. This can be explained by the added polarizability of the metal split ring resonators.

In Fig. 6, the measured blockages are consistently lower than the simulated ones, due to the slightly larger frequency interval obtained in the simulations. The only exception is at 45°, where the measured TE results exceed the simulations. This indicates that the measurement setup was probably perturbed at this point, but the results remain below the bound, and this observation does not change the conclusions in this paper.

6 Conclusions

By generalizing results from [11] we have derived a bound on the all-spectrum transmission blockage through a low-pass periodic screen for oblique incidence in (3.9). The result is that the transmission blockage is bounded by the sum of the electric and magnetic polarizabilities per unit area of the screen, with an angular dependence corresponding to the transverse components of the incident field. The bounds

were demonstrated theoretically and experimentally using nonmagnetic structures, and it was seen that a composite structure with metal patterns like split ring resonators on a dielectric substrate can increase the transmission blockage by an order of magnitude compared to the pure dielectric substrate.

For a nonmagnetic structure, the polarizability in (3.8) for TM polarization is usually lower than the polarizability at high angles of incidence. This is due to the longitudinal polarizability γ_{ezz} usually being smaller than the transverse polarizability $\boldsymbol{\gamma}_{\mathrm{ett}}$. The transverse electric polarizability can be associated with the low-frequency shunt capacitance of the sheet [23]. Since the bounds are proportional to this factor, we have presented a theoretical basis for the rule-of-thumb that in order to construct a band-stop frequency selective screen with high bandwidth, it is a good idea to use elements with high capacitive mutual coupling [15]. The dependence on angle was shown to be more severe for TM polarization, which is also observed in practice. For TM polarization the longitudinal polarizability γ_{ezz} can be associated with the low frequency series inductance of the sheet [23], implying that further gain in bandwidth for TM polarization might be achieved by increasing the equivalent series inductance of the sheet. This can be done both by increasing γ_{ezz} (for instance by loading the structure with metal pins in the z direction), and by increasing $\boldsymbol{\gamma}_{\mathrm{mtt}}$ (by using magnetic materials).

From the example of the dielectric sheet, it is seen that the high-frequency delay can have a substantial influence on the bound. Since our measurements are always band limited, this parameter can only be determined by extrapolating the measurement data, or bounded below by zero.

7 Acknowledgments

The financial support by the Swedish Foundation for Strategic Research is gratefully acknowledged.

References

[1] A. Bernland, A. Luger, and M. Gustafsson. Sum rules and constraints on passive systems. Technical Report LUTEDX/(TEAT-7193)/1-31/(2010), Lund University, Department of Electrical and Information Technology, P.O. Box 118, S-221 00 Lund, Sweden, 2010. `http://www.eit.lth.se`.

[2] F. Bloch. Über die Quantenmechanik der Electronen in Kristallgittern. *Z. Phys.*, **52**, 555–600, 1928.

[3] M. Born and E. Wolf. *Principles of Optics.* Cambridge University Press, Cambridge, U.K., seventh edition, 1999.

[4] C. R. Brewitt-Taylor. Limitation on the bandwidth of artificial perfect magnetic conductor surfaces. *Microwaves, Antennas & Propagation, IET*, **1**(1), 255–260, 2007.

[5] R. M. Fano. Theoretical limitations on the broadband matching of arbitrary impedances. *Journal of the Franklin Institute*, **249**(1,2), 57–83 and 139–154, 1950.

[6] G. Floquet. Sur les équations différentielles linéaries à coefficients périodique. *Ann. École Norm. Sup.*, **12**, 47–88, 1883.

[7] M. Gustafsson and D. Sjöberg. Sum rules and physical bounds on passive metamaterials. *New Journal of Physics*, **12**, 043046, 2010.

[8] M. Gustafsson, C. Sohl, and G. Kristensson. Physical limitations on antennas of arbitrary shape. *Proc. R. Soc. A*, **463**, 2589–2607, 2007.

[9] M. Gustafsson, C. Sohl, and G. Kristensson. Illustrations of new physical bounds on linearly polarized antennas. *IEEE Trans. Antennas Propagat.*, **57**(5), 1319–1327, May 2009.

[10] M. Gustafsson. Sum rule for the transmission cross section of apertures in thin opaque screens. *Opt. Lett.*, **34**(13), 2003–2005, 2009.

[11] M. Gustafsson, C. Sohl, C. Larsson, and D. Sjöberg. Physical bounds on the all-spectrum transmission through periodic arrays. *EPL Europhysics Letters*, **87**(3), 34002 (6pp), 2009.

[12] D. S. Jones. Scattering by inhomogeneous dielectric particles. *Quart. J. Mech. Appl. Math.*, **38**, 135–155, 1985.

[13] C. Kittel. *Introduction to Solid State Physics.* John Wiley & Sons, New York, 7 edition, 1996.

[14] G. Kristensson, S. Poulsen, and S. Rikte. Propagators and scattering of electromagnetic waves in planar bianisotropic slabs — an application to frequency selective structures. *Progress in Electromagnetics Research*, **48**, 1–25, 2004.

[15] B. Munk. *Frequency Selective Surfaces: Theory and Design.* John Wiley & Sons, New York, 2000.

[16] H. M. Nussenzveig. *Causality and dispersion relations.* Academic Press, London, 1972.

[17] S. J. Orfanidis. Electromagnetic waves and antennas, 2002. `www.ece.rutgers.edu/~orfanidi/ewa`, revision date June 21, 2004.

[18] K. N. Rozanov. Ultimate thickness to bandwidth ratio of radar absorbers. *IEEE Trans. Antennas Propagat.*, **48**(8), 1230–1234, August 2000.

[19] B. E. A. Saleh and M. C. Teich. *Fundamentals of Photonics.* John Wiley & Sons, New York, 1991.

[20] D. Sjöberg. Homogenization of dispersive material parameters for Maxwell's equations using a singular value decomposition. *Multiscale Modeling and Simulation*, **4**(3), 760–789, 2005.

[21] D. Sjöberg. Low frequency scattering by passive periodic structures for oblique incidence: low pass case. *J. Phys. A: Math. Theor.*, **42**, 385402, 2009.

[22] D. Sjöberg. Variational principles for the static electric and magnetic polarizabilities of anisotropic media with perfect electric conductor inclusions. *J. Phys. A: Math. Theor.*, **42**, 335403, 2009.

[23] D. Sjöberg. Circuit analogs for wave propagation in stratified structures. In A. Petrin, editor, *Wave Propagation in Materials for Modern Applications*, pages 489–508. InTech, 2010.

[24] D. Sjöberg, C. Engström, G. Kristensson, D. J. N. Wall, and N. Wellander. A Floquet-Bloch decomposition of Maxwell's equations, applied to homogenization. *Multiscale Modeling and Simulation*, **4**(1), 149–171, 2005.

[25] J. Skaar and K. Seip. Bounds for the refractive indices of metamaterials. *J. Phys. D: Applied Phys.*, **39**(6), 1226, 2006.

[26] C. Sohl, M. Gustafsson, and G. Kristensson. Physical limitations on broadband scattering by heterogeneous obstacles. *J. Phys. A: Math. Theor.*, **40**, 11165–11182, 2007.

[27] C. Sohl, M. Gustafsson, and G. Kristensson. Physical limitations on metamaterials: Restrictions on scattering and absorption over a frequency interval. *J. Phys. D: Applied Phys.*, **40**, 7146–7151, 2007.

[28] C. Sohl, C. Larsson, M. Gustafsson, and G. Kristensson. A scattering and absorption identity for metamaterials: experimental results and comparison with theory. *J. Appl. Phys.*, **103**(5), 054906, 2008.

[29] R. Yang, Y. J. Xie, X. F. Li, Y. Y. Wang, R. Wang, and J. Jiang. Causality in the resonance behavior of metamaterials. *EPL (Europhysics Letters)*, **84**(3), 34001 (6pp), 2008.